

Plaquette-centered rotation symmetry and octet-nodal superconductivity in KFe_2As_2

Guo-Yi Zhu¹ and Guang-Ming Zhang^{1,2}

¹*State Key Laboratory of Low-Dimensional Quantum Physics and*

Department of Physics, Tsinghua University, Beijing 100084, China.

²*Collaborative Innovation Center of Quantum Matter, Beijing 100084, China.*

(Dated: November 10, 2018)

A plaquette-centered rotation symmetry C_4^p is identified to play a significant role in determining and stabilizing the Fermi-surface structure of Fe-based superconductors. Together with the S_4 symmetry previously found, we are able to sort out the tangling orbitals and solve the puzzle of pairing symmetry of superconductivity in KFe_2As_2 in a simple but comprehensive way. By modeling the material with a strong coupling $t - J_1 - J_2$ model, we find phase transitions of pairing symmetry driven by the competition between the local spin antiferromagnetic couplings from nodal $d_{x^2-y^2} \times s_{x^2+y^2}$ -wave to nodeless $s_{x^2-y^2}$ -wave through the intermediate $s + id \times s$ mixed pairing phase, which is consistent with the observation of pressure experiments. The emergent d -wave form factor inevitably arises from the projection of inter-orbital Cooper pairing onto the Fermi surface and is inherited from the electronic structure in the representation of C_4^p symmetry. Moreover, the S_4 symmetry dictates 2 copies of d -wave pairing condensates, counting 8 nodes in total. We further show that weakly breaking C_4^p naturally leads to the octet nodal gap as precisely observed in laser angle resolved photoemission spectroscopy. The octet nodes reflect the collaboration of the C_4^p and S_4 symmetries, which sheds new light on the enigma of the pairing symmetry in KFe_2As_2 .

As the first family of high temperature superconductivity (SC), the cuprates have been under elaborate studies for nearly thirty years[1–4], and a consensus has been reached by the majority of condensed matter physicists that the intriguing superconducting phase of cuprates are rooted in the electronic strong antiferromagnetic (AF) correlation. The SC in optimally doped compounds is confirmed by a vast majority experiments to be d -wave pairing symmetry[5–7]. For the theorists, the complex reality arising from both the $3d$ orbital on Cu ions and $2p$ orbital on O ions is compromised by formation of the Zhang-Rice singlets, which justifies a rather successful description of a single-band model for the cuprates - the celebrated t-J model[3, 4, 8–10].

The phase diagrams of Fe-based superconductors show significant similarity with those of the cuprates, suggesting deep connection of the essential physics between them. However, distinct from the cuprates, the family of Fe-based superconductors has a seemingly less unified picture as to their Fermi surface (FS) structure, pairing symmetries and pairing glues[11–16]. From the perspective of band structure, they owe their complexity to the multi-orbital character. Some Fermi pockets could vanish under doping or pressure and are less robust than the others[17, 18]. Regarding the pairing symmetry, the s_{\pm} -wave pairing symmetry has been established for many iron-pnictides from different approaches[19–21], but it fails to account for all the materials observed experimentally. When it comes to the interactions responsible for pairing, there are weak coupling theories that count on the antiferromagnetic spin fluctuation[19], but they are less satisfying when FS nesting is absent, nor when there exists strong correlation between local magnetic moments[11–16]. After all these considerations, a simple but unifying theoretical recipe for the Fe-based

superconductors is still elusive, and we still need deep reflection upon the electronic structure and interactions of Fe-based superconductors.

To model the Fe-based SCs, we have to firstly understand the electronic structure. There have been many theoretical treatments by taking all five or even ten $3d$ -orbitals of Fe into consideration, but the necessity for such a huge parameter space is hardly conceivable, because the pairing symmetries are so robust. From this point of view, we especially appreciate the S_4 symmetry found by Hu and Hao[22], which provides a rational way to sort out the tangling multi-orbitals of Fe-based SCs and reduce the parameters of the electronic structure. In the presence of S_4 , the band structure of multi-orbitals is then reduced to a minimal two-band model. Based on this S_4 symmetry, the model with a few parameters is capable of accommodating most FS structures of both iron-pnictides and iron-chalcogenides[22], potentially unifying the electronic structure of Fe-based SCs. However, the heavily hole doped limit of iron-pnictides KFe_2As_2 is left behind.

The representative of heavily hole doped $\text{Ba}_{1-x}\text{K}_x\text{Fe}_2\text{As}_2$ family - KFe_2As_2 is a particular intriguing case among the Fe-based superconductors, regarding its pairing symmetry and interaction. Angle resolved photoemission spectroscopy (ARPES) experiments[17, 18] report the absence of electron pockets and leave only three hole Fermi pockets around the Brillouin zone (BZ) center (Γ point). Usually the nodeless s -wave pairing symmetry is favorable. But it turns out that nodal gap structure was observed by thermal conductivity measurement[23], penetration depth measurement[24], and NMR probe[25–27]. The d -wave pairing symmetry was then proposed after functional renormalization group calculation[28], which seems

consistent with the measurement of heat conduction[29]. Later on Okazaki et. al. utilized the ultra-high energy resolution of laser ARPES to map the gap structure much more explicitly[30]. Quite dramatically, their report showed octet nodal gap on the middle hole pocket while nodeless gap on the inner hole pocket, in striking contrast to the theoretical expectation. Then there were attempts to resort to accidental nodes to account for the octet nodes. But as far as we are concerned, the nodes robustly observed in various experiments deserve far more convincing explanation. If the octet nodes was given by an effective g-wave pairing condensate phenomenologically, it is a natural question how the Cooper pair obtains angular momentum as high as $l = 4$ microscopically. Although the so-called concealed d-wave scenario was proposed to explain the formation of the effective g-wave Cooper pair, such a theory starts from an orbital selective pairing form, and their orbital triplet pairing vector field is required to be locked with the orbital Rashba vector field and to rotate oppositely[31].

In this paper, we will provide a mechanism based on a microscopic minimal model, which is much simpler but more transparent. Our idea is inspired by another experiment. Taillefer's group reported their pressure study on KFe_2As_2 , in which they witnessed a non-monotonic V-shaped tendency of the superconducting transition temperature with increasing pressure[32]. Their results clearly indicated a phase transition near the point of the sudden change of T_c . The possibility of FS transition was ruled out by their Hall coefficient measurement, pointing towards a phase transition of pairing symmetry. It should be emphasized that the KFe_2As_2 is regarded as a strongly correlated system with strong AF fluctuation evidenced by the remarkable mass enhancement[17, 33] and high incoherent spectral weight[34]. Since the main ingredients determining the pairing symmetry are the FS structure and the electronic interactions responsible for pairing, it can be concluded that the phase transitions are essentially driven by the competition between the local spin AF exchanges, because the FS remains almost the same.

First of all, we identify a plaquette-centered rotation symmetry C_4^p which is complementary to the S_4 symmetry, providing a simple and potentially universal organizing principle for the tangling orbitals of Fe-based superconductors. We explicitly show that, while S_4 plays the role of organizing two groups of orbitals, C_4^p is responsible for determining and stabilizing the FS structure of iron-pnictides, including the heavily hole doped limit where the electron Fermi pockets are absent. The joint cooperation of the S_4 and C_4^p symmetries manifest its power particularly in settling the controversy of pairing symmetry and nodeness in KFe_2As_2 .

To study the pairing symmetry of SC in KFe_2As_2 , we take the strong coupling approach by modeling this ma-

terial with the $t - J_1 - J_2$ model subjected to the particle occupancy constraint, in contrast to the models with the on-site Coulomb repulsion and Hund's coupling[35]. Since we are mainly concerned with the pairing symmetry of superconductivity, we can neglect the quantum fluctuation for the moment and adopt the slave-boson mean-field approximation. We find that, by decreasing the ratio of J_1/J_2 , the KFe_2As_2 samples could experience phase transitions of pairing symmetry from the $d_{x^2-y^2} \times s_{x^2+y^2}$ -wave SC to $s_{x^2-y^2}$ -wave SC through a narrow intermediate $s+id \times s$ mixed pairing phase. Although the d -wave pairing symmetry is indeed energetically unfavorable compared with the s -wave pairing, the electronic structure imposes an indispensable d -wave form factor on the Cooper pairs glued by the local spin AF coupling J_1 . This d -wave form factor is inherited from the orbital hybridization in the representation of C_4^p and becomes the characteristic nature of multi-orbital iron-pnictide superconductors. Moreover, together with the S_4 symmetry, we are in fact bestowed with 2 copies of d -wave gap structure, counting 8 nodes in total. By weakly breaking C_4^p we are naturally led to the so-called "octet-noded monster" observed by laser ARPES. We thus propose a symbolic equation "8 = 4 + 4" that captures the essential physics ruled by S_4 and C_4^p symmetries, exhibiting the origin of nodes in a rather simple and comprehensive way.

Moreover, we find that a different representation of this plaquette-centered rotation symmetry \tilde{C}_4^p can stabilize the FS structure of iron-chalcogenides, including the monolayer FeSe on SrTiO_3 substrate where a tiny hole Fermi pocket around Γ vanishes[36, 37]. So both families of Fe-based superconductors share the plaquette-centered rotation symmetry, and the importance of this symmetry lies in its capability to understand the band topology and robustness of FSs, and to reconcile some seemingly contradictory experimental observations in a rather simple, inevitable, and comprehensive manner.

RESULTS

C_4^p symmetry and band topology

Due to the weak out-of-plane coupling (along c-axis), the electronic properties of Fe-based SCs are mainly contained in the FeAs plane, where the Fe atoms form a square lattice and the As atoms alternate above or below the Fe plaquette center (Fig.1a). Because of the checkerboard pattern of As lattice, the FeAs plane does not respect the site-centered C_4^s symmetry, but is invariant under the site-centered C_4^s rotation followed by a mirror reflection with respect to the plane[22]: $S_4 \equiv C_4^s \times R_z$. We further discover that the plaquette-centered rotation symmetry C_4^p is preserved.

Among the five d -orbitals, the low-energy physics near the FS is mainly contributed by the d_{xz}, d_{yz}, d_{xy} orbitals. Instead of a direct tunneling via the wave function over-

lap, the hopping between d_{xz} - and d_{yz} -orbitals is primarily contributed by their hybridization with the p -orbitals on the As atoms, whereas the d_{xy} orbitals do not have this privilege and are not included in our minimal model. The As atoms on plaquette centers polarize the d_{xz} - and d_{yz} -orbitals into $d_{x'z}$ - and $d_{y'z}$ -orbitals to maximize energy gain from hopping (Fig.1a and Fig.1b). Therefore the square lattice with $d_{x'z}$ and $d_{y'z}$ orbitals on each site is effectively factorized into the top and bottom layers where each site has one orbital but the unit cell has to be doubled. As shown in Fig.1b, the top layer has $d_{x'z}$ living on the odd lattice sites (denoted as A) and $d_{y'z}$ on the even lattice sites (denoted as B). Likewise, the bottom layer has $d_{y'z}$ living on the odd lattice sites (denoted as C) and $d_{x'z}$ on the even lattice sites (denoted as D). For convenience we will denote the top layer as "AB layer" while the bottom layer as "CD layer". Albeit weakly coupled by inter-layer tunneling, the two layers are related by the S_4 symmetry, while the sublattice degrees of freedom inside each layer are rotated by C_4^p .

To demonstrate the symmetries, we introduce the notation $\tau_{\mu\nu} \equiv I_\mu \otimes I_\nu$, $\mu, \nu = 0, 1, 2, 3$, where the first Pauli matrix I_μ acts on the S_4 spinor space spanned by those states living on either layer, and the latter Pauli matrix I_ν acts on the C_4^p spinor space composed of states living on each sublattice. By choosing the simple gauge as shown in Fig.1b, the representation of S_4 and C_4^p symmetries can be explicitly expressed as

$$S_4 : \begin{pmatrix} A_{\mathbf{k},\sigma} \\ B_{\mathbf{k},\sigma} \\ C_{\mathbf{k},\sigma} \\ D_{\mathbf{k},\sigma} \end{pmatrix} \rightarrow \begin{pmatrix} C_{\mathbf{k}',\sigma} \\ -D_{\mathbf{k}',\sigma} \\ -A_{\mathbf{k}',\sigma} \\ B_{\mathbf{k}',\sigma} \end{pmatrix} = i\tau_{23} \begin{pmatrix} A_{\mathbf{k}',\sigma} \\ B_{\mathbf{k}',\sigma} \\ C_{\mathbf{k}',\sigma} \\ D_{\mathbf{k}',\sigma} \end{pmatrix},$$

$$C_4^p : \begin{pmatrix} A_{\mathbf{k},\sigma} \\ B_{\mathbf{k},\sigma} \\ C_{\mathbf{k},\sigma} \\ D_{\mathbf{k},\sigma} \end{pmatrix} \rightarrow \begin{pmatrix} B_{\mathbf{k}',\sigma} \\ -A_{\mathbf{k}',\sigma} \\ -D_{\mathbf{k}',\sigma} \\ C_{\mathbf{k}',\sigma} \end{pmatrix} = i\tau_{32} \begin{pmatrix} A_{\mathbf{k}',\sigma} \\ B_{\mathbf{k}',\sigma} \\ C_{\mathbf{k}',\sigma} \\ D_{\mathbf{k}',\sigma} \end{pmatrix},$$

where $\mathbf{k}' = C_4 \mathbf{k}$. Since the spin-orbit coupling is not concerned, the spin degeneracy is always present. The rotation factor contributed by the spin rotation $(1 + i\sigma_z)/\sqrt{2}$ does not affect the physics and can be absorbed by a basis transformation. Moreover, we would like to point out that these two symmetries commute with each other.

Formally, the C_4^p symmetry operation is indeed diagonal in the S_4 spinor space and mainly rotates the intra-layer sublattices, while the S_4 operation is diagonal in each sublattice but primarily rotates the layers. It is worth noticing that the S_4 spinor and C_4^p spinor look like dual to each other. But the inter-sublattice hopping is much stronger than the inter-layer tunneling, which makes the S_4 doublet weakly coupled but C_4^p doublet strongly hybridized. The power of the S_4 symmetry lies in that, once the dynamics of one layer is obtained, it is straightforward to derive the other. Therefore, in the presence of S_4 symmetry, we are bestowed with a minimal

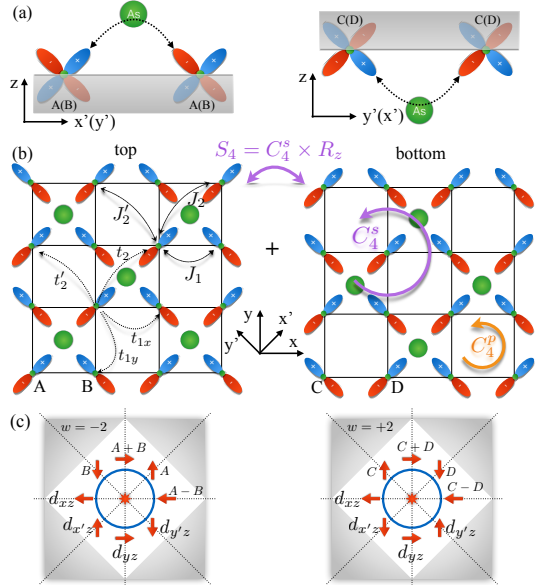


FIG. 1: Lattice configuration of the iron-pnictides. (a) The transverse view of the Fe-As plane shows the hopping of $3d_{x'(y')z}$ orbital via hybridization with $p_{x'(y')}$ orbital on arsenic atoms, either above or below the Fe square lattice plane. (b) The $3d_{x'(y')z}$ orbitals on the Fe lattice can be approximately decoupled into two groups which hop around via the arsenic atom on top or bottom of the plane respectively. Thus the lattice can be viewed as "factorized" into the top and bottom layers, which are related by S_4 symmetry. (c) For d -wave representation of plaquette-centered rotation symmetry C_4^p , the Γ point is the source of Berry flux carrying topological winding number $w = \mp 2$ for AB (CD) layer. The red arrow denotes the polarization of C_4^p spinor on the Fermi pocket, where spin up represents A(C) orbitals and spin down represents B(D) orbitals.

C_4^p spinor model living on either layer. In the following we focus on the properties of the top layer before paying a revisit to the complete S_4 spinor.

As shown in Fig.1b, the kinetic part of the model Hamiltonian mainly involves anisotropic nearest neighbor (NN) hopping t_1 and the next nearest neighbor (NNN) hopping t_2 or t'_2 , which can be recombined and decomposed into s -wave and d -wave representation: $t_{1s} = (t_{1x} + t_{1y})/2$, $t_{1d} = (t_{1x} - t_{1y})/2$, $t_{2s} = (t_2 + t'_2)/2$, and $t_{2d} = (t_2 - t'_2)/2$. In terms of the C_4^p spinor $\Psi_{\mathbf{k},\sigma} \equiv (A_{\mathbf{k},\sigma}, B_{\mathbf{k},\sigma})^T$, it is then expressed as

$$H_t^{\text{AB}} = \frac{1}{2} \sum_{\mathbf{k},\sigma} \Psi_{\mathbf{k},\sigma}^\dagger [\epsilon_0(\mathbf{k}) + \epsilon_x(\mathbf{k})I_1 + \epsilon_z(\mathbf{k})I_3] \Psi_{\mathbf{k},\sigma}, \quad (1)$$

where \mathbf{k} ranges in the unfolded BZ and

$$\begin{aligned} \epsilon_0(\mathbf{k}) &= 4t_{2s} \cos k_x \cos k_y - \mu, \\ \epsilon_z(\mathbf{k}) &= -4t_{2d} \sin k_x \sin k_y, \\ \epsilon_x(\mathbf{k}) &= 2t_{1d} (\cos k_x - \cos k_y) + 2t_{1s} (\cos k_x + \cos k_y) \\ &\equiv \epsilon_{xd}(\mathbf{k}) + \epsilon_{xs}(\mathbf{k}). \end{aligned}$$

Note that $\epsilon_z(\mathbf{k})$ denotes the sublattice energy difference and $\epsilon_x(\mathbf{k})$ is the energy gain from the NN hopping process. A vector can be defined by $\mathbf{h}(\mathbf{k}) \equiv (\epsilon_x, 0, \epsilon_z)$, which acts as a "magnetic field" in the momentum space and pinning the C_4^p spinor (Fig.1c). It should be noted that the sublattice degree of freedom in AB layer is locked with the atomic internal angular momentum i.e. the odd sites carry $d_{x'z}$ orbitals while the even sites carry $d_{y'z}$ orbitals, so that the C_4^p spinor is actually a composite of the sublattice degree of freedom and the internal atomic angular momentum. For instance, when $t_{1s} = 0$, $t_{1d} < 0$, $t_{2s} > 0$, and $t_{2d} > 0$, the spinor along k_x with the lowest energy is composed of the equal superposition of $d_{x'z}$ -orbitals on odd sites and $d_{y'z}$ -orbitals on even sites (Fig.1c), equivalent to d_{xz} -orbitals. But along the BZ diagonal, the spinor with the lowest energy consists of the $d_{x'z}$ -orbitals on odd sites or $d_{y'z}$ -orbitals on even sites.

Before diagonalization, there are several remarks about the symmetries in this kinetic part. The d -wave and s -wave NN hopping correspond to two distinctive symmetry representations of the plaquette-centered rotation symmetry, respectively. Based on the sketch of a snapshot of the wave function distribution in Fig.1b, we naturally expect $|t_{1d}| \gg |t_{1s}| \approx 0$. Indeed, adding a nonzero t_{1s} would break the symmetry C_4^p . So the ideal case of $t_{1s} = 0$ and $t_{1d} \neq 0$ respects the symmetry C_4^p , which can faithfully characterize the FS structure of iron-pnictides.

In the helicity basis, H_t^{AB} can be directly diagonalized

$$H_t^{\text{AB}} = \frac{1}{2} \sum_{\mathbf{k},\sigma} \left[\xi_e(\mathbf{k}) \alpha_{\mathbf{k},\sigma}^\dagger \alpha_{\mathbf{k},\sigma} + \xi_h(\mathbf{k}) \beta_{\mathbf{k},\sigma}^\dagger \beta_{\mathbf{k},\sigma} \right], \quad (2)$$

where $\xi_{e(h)}(\mathbf{k}) = \epsilon_0 \pm \sqrt{\epsilon_x^2 + \epsilon_z^2}$ represents the electron (hole) band with \pm helicity, respectively:

$$\begin{aligned} \alpha_{\mathbf{k},\sigma}^\dagger &= \left(\cos \frac{\theta_{\mathbf{k}}}{2} \right) A_{\mathbf{k},\sigma}^\dagger + \text{sgn}(\epsilon_x) \left(\sin \frac{\theta_{\mathbf{k}}}{2} \right) B_{\mathbf{k},\sigma}^\dagger, \\ \beta_{\mathbf{k},\sigma}^\dagger &= \left(\cos \frac{\theta_{\mathbf{k}}}{2} \right) B_{\mathbf{k},\sigma}^\dagger - \text{sgn}(\epsilon_x) \left(\sin \frac{\theta_{\mathbf{k}}}{2} \right) A_{\mathbf{k},\sigma}^\dagger, \end{aligned} \quad (3)$$

and the hybridization angle is given by $\theta_{\mathbf{k}} = \tan^{-1} \frac{|\epsilon_x|}{\epsilon_z} \in [0, \pi]$. The band dispersion and the corresponding FS structures can be easily obtained. Fig.2a exhibits the coexistence of a hole pocket around Γ and an electron pocket around X point in the absence of the s -wave NN hopping, a characteristic FS structure of most iron-pnictides. As the d -wave NN hopping is growing, the electron band is gradually pushed upwards, shrinking the electron pocket. It finally leads to the FS structure of KFe_2As_2 (Fig.2b), where the electron pocket completely vanishes. This evolution is also related to the doping process of $\text{Ba}_{1-x}\text{K}_x\text{Fe}_2\text{As}_2$ iron-pnictides[39].

Note that the shape of the hole pocket has the C_4 rotational symmetry thanks to the symmetry C_4^p , and the

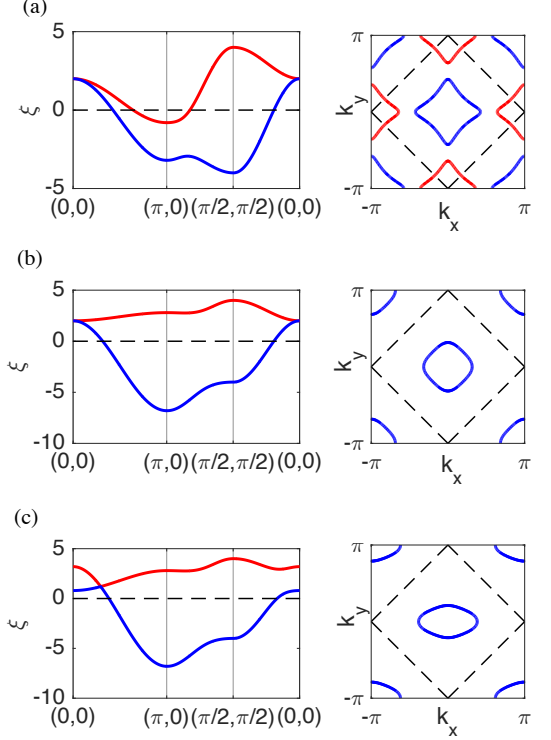


FIG. 2: Band structures and Fermi surfaces of the minimal model without considering any electron interactions for various systems of Fe-based superconductors. Left panel shows the band structure for varying parameters while right panel shows the corresponding FS in the unfolded BZ. (a) The parameters are $t_{1d} = -0.3$, $t_{1s} = 0$, $t_{2s} = 0.5$, in unit of $t_{2d} = 1$. Hole pocket is located around Γ and electron pocket around X , describing the FS structure for iron-pnictides. The Γ point is a double Dirac point with quadratic band touching dispersion. (b) The parameters are $t_{1d} = -1.2$, $t_{1s} = 0$, $t_{2s} = 0.5$, in unit of $t_{2d} = 1$. Electron pocket vanishes, while the hole pocket around Γ is robust, standing for the heavily hole doped iron-pnictides. (c) The parameters are $t_{1d} = -1.2$, $t_{1s} = -0.3$, $t_{2s} = 0.5$, in unit of $t_{2d} = 1$. Mixing d -wave NN hopping with s -wave component can split the double Dirac point into two Dirac points while elongating the hole pocket. Hole pocket could be further torn apart.

two bands touch each other quadratically at zone center Γ point, which is not accidental but rather due to the topological nature. Namely, the helical spinor is pinned by the vector field $\mathbf{h}(\mathbf{k})$ to wind around the Γ point twice, yielding a topological number $w = 2\text{sgn}(t_{1d}t_{2d})$ (Ref.[40]). It is this topological number that forces the electron and hole bands to touch quadratically at the vortex core of $\mathbf{h}(\mathbf{k})$, which becomes the source of the Berry flux experienced by the helical spinor (see Fig.1c). Consequently, the hole pocket surrounding the vortex core is protected by topology, whereas the electron pocket is less robust. As long as the time reversal (TR) symmetry is present, the occurrence of I_2 is forbidden and this vortex core is robust. However, the TR symmetry cannot prevent the double Dirac point at Γ from splitting apart into

two separated Dirac nodes, which could be driven by a weak C_4^p -breaking perturbation. This is indeed the case when the s -wave hoping comes in mixing the d -wave NN hopping (Fig.2c), where the hole pocket experiences a "nematic force" and is simultaneously elongated. When the C_4^p symmetry breaking term is large enough, the hole pocket around Γ is going to be torn apart, resulting in two pockets surrounding the Dirac nodes, which is not seen in the real materials. So the iron-pnictides with hole pockets around Γ robustly observed in experiments must preserve the C_4^p symmetry, at least approximately. In other words, the FS structure of iron-pnictides is stabilized by the C_4^p symmetry which helps the TR symmetry protect and confine the double Dirac point to the hole pocket center. In this sense, the C_4^p symmetry is one of the key relevant features of iron-pnictides, which can tolerate only tiny amount of s -wave hopping. In the next section, we will focus on the ideal case of d -wave NN hopping limit by sending $t_{1s} \rightarrow 0$ for KFe_2As_2 . Specifically, we choose the realistic hopping parameters as $t_{1d} = -1.2$, $t_{2s} = 0.5$, and $t_{2d} = 1$, whose corresponding band structure is given by Fig.2b. When things are clear in the ideal case, we will introduce a weak s -wave NN hopping to model the more realistic material later on.

C_4^p protected d -wave renormalized pairing SC

Provided the electronic structure of KFe_2As_2 , we need to include the electronic interactions. The strong correlation evidenced by experiments[17, 33, 34] requires a strong coupling approach. Particularly, the optical measurement[34] had showed the incoherent spectral weight of KFe_2As_2 as high as 10% hole-doped $\text{La}_{2-x}\text{Sr}_x\text{CuO}_4$, revealing the strong local AF correlation similar to the cuprates. Therefore, we would like to model this system with AF super-exchanges containing the NN and NNN interactions as shown in Fig.1b. Distinct from the $t - J_1 - J_2$ model in the previous form[20], our model Hamiltonian is subjected to a constraint that projects out double-occupancy. Thus, the model Hamiltonian for AB layer is described by $H_t^{\text{AB}} = \mathcal{P}H_t^{\text{AB}}\mathcal{P} + H_J^{\text{AB}}$ with interaction terms:

$$H_J^{\text{AB}} = J_1 \sum_{\mathbf{r}, \delta} S_{\mathbf{r}}^A \cdot S_{\mathbf{r}+\delta}^B + J_2 \sum_{\mathbf{r}} \left(S_{\mathbf{r}}^A \cdot S_{\mathbf{r}+(\hat{x}+\hat{y})}^A + S_{\mathbf{r}}^B \cdot S_{\mathbf{r}+(\hat{x}-\hat{y})}^B \right) + J'_2 \sum_{\mathbf{r}} \left(S_{\mathbf{r}}^A \cdot S_{\mathbf{r}+(\hat{x}-\hat{y})}^A + S_{\mathbf{r}}^B \cdot S_{\mathbf{r}+(\hat{x}+\hat{y})}^B \right), \quad (4)$$

where $\delta = \pm \hat{x}, \hat{y}$ is the NN vector. As the low-energy descendant of the on-site Hubbard interaction, the AF super-exchange J -terms rely on the corresponding hopping integrals. Like cuprates, the parameters can be chosen as $J_2 = 0.5$ and $J'_2 = 0.2$ as roughly one third of the corresponding hopping integrals and the dopant concentration is fixed at 0.05. Note that although J'_2 differs from J_2 , only the combination $J_{2s} \equiv 2J_2J'_2/(J_2 + J'_2)$

contributes to pairing. So that the physics is essentially captured by the competition between J_1 and J_{2s} . The parameter J_1 is chosen as the tuning parameter that mimics the inverse pressure when compared with the pressure experiments[32].

The projector \mathcal{P} declares the particle occupancy constraints: $\sum_{\sigma} A_{\mathbf{r},\sigma}^\dagger A_{\mathbf{r},\sigma} \leq 1$ and $\sum_{\sigma} B_{\mathbf{r},\sigma}^\dagger B_{\mathbf{r},\sigma} \leq 1$, which lead to emergent spin-charge separation physics. To tackle the constraint, we adopt the well-established slave-boson decomposition to factorize electron into fermionic spinon and bosonic holon:

$$A_{\mathbf{r},\sigma} = h_{\mathbf{r}}^\dagger a_{\mathbf{r},\sigma}, B_{\mathbf{r},\sigma} = h_{\mathbf{r}}^\dagger b_{\mathbf{r},\sigma}, \quad (5)$$

in which way the constraint becomes equalities: $\sum_{\sigma} a_{\mathbf{r},\sigma}^\dagger a_{\mathbf{r},\sigma} + h_{\mathbf{r}}^\dagger h_{\mathbf{r}} = 1$ and $\sum_{\sigma} b_{\mathbf{r},\sigma}^\dagger b_{\mathbf{r},\sigma} + h_{\mathbf{r}}^\dagger h_{\mathbf{r}} = 1$, and can be enforced via a Lagrangian multiplier. After the bosonic holons are condensed $\langle h_{\mathbf{r}}^\dagger \rangle = \langle h_{\mathbf{r}} \rangle = \sqrt{x}$, we introduce the uniform valence bond and singlet pairing order parameters

$$\kappa_{ij} = -\frac{J}{4} \left\langle \sum_{\sigma} a_{i,\sigma}^\dagger a_{j,\sigma} \right\rangle, \Delta_{ij} = \frac{J}{4} \langle a_{i,\uparrow} a_{j,\downarrow} - a_{i,\downarrow} a_{j,\uparrow} \rangle,$$

to decouple the local AF interactions. Moreover, the NN and NNN valence bond and singlet pairing order parameters in real space can be rearranged into the s -wave and d -wave representations: κ_1 is automatically of d -wave symmetry required by C_4^p symmetry and other valence bond orders are

$$\begin{aligned} \kappa_{2s} &= (\kappa_2 + \kappa'_2)/2, \kappa_{2d} = (\kappa_2 - \kappa'_2)/2, \\ \Delta_{1s} &= (\Delta_{1x} + \Delta_{1y})/2, \Delta_{1d} = (\Delta_{1x} - \Delta_{1y})/2, \\ \Delta_{2s} &= (\Delta_2 + \Delta'_2)/2, \Delta_{2d} = (\Delta_2 - \Delta'_2)/2. \end{aligned} \quad (6)$$

Finally, a mean-field Hamiltonian can be obtained

$$H_{\text{MF}}^{\text{ab}} = H_t^{\text{ab}} + H_{\Delta}^{\text{ab}}, \quad (7)$$

which describes the superconducting quasiparticles on the AB layer. The kinetic part H_t^{ab} has the same band structure as we discussed in the last section. $H_t^{\text{AB}} \rightarrow H_t^{\text{ab}}$ requires replacing the electrons with the corresponding quasiparticles $\Psi_{\mathbf{k},\sigma} = (A_{\mathbf{k},\sigma}, B_{\mathbf{k},\sigma})^T \rightarrow \psi_{\mathbf{k},\sigma} \equiv (a_{\mathbf{k},\sigma}, b_{\mathbf{k},\sigma})^T$, while renormalizing the hopping integrals and the chemical potential as

$$\begin{aligned} t_{1d} &\rightarrow \tilde{t}_{1d} = (t_{1d}x + \kappa_1), \quad t_{1s} \rightarrow \tilde{t}_{1s} = t_{1s}x, \\ t_{2s} &\rightarrow \tilde{t}_{2s} = (t_{2s}x + \kappa_{2s}), \\ t_{2d} &\rightarrow \tilde{t}_{2d} = (t_{2d}x + \kappa_{2d}), \\ \mu_0 &\rightarrow \mu = \mu_0 - \lambda - (J_2 + J_3)/4. \end{aligned} \quad (8)$$

The hybridization relation Eq. (3) also holds by replacing A(B) with a(b), and the mean-field pairing terms can be compactly expressed in terms of the C_4^p spinor:

$$H_{\Delta}^{\text{ab}} = \frac{1}{2} \sum_{\mathbf{k}} \left[\psi_{\mathbf{k},\uparrow}^\dagger (\Delta_0 + i\Delta_x I_x + \Delta_z I_z) (\psi_{\mathbf{k},\downarrow}^\dagger)^T + h.c. \right] \quad (9)$$

with

$$\begin{aligned}\Delta_0(\mathbf{k}) &= 4\Delta_{2s} \cos k_x \cos k_y, \Delta_z(\mathbf{k}) = 4\Delta_{2d} \sin k_x \sin k_y, \\ \Delta_x(\mathbf{k}) &= 2\Delta_{1s} (\cos k_x + \cos k_y) + i2\Delta_{1d} (\cos k_x - \cos k_y).\end{aligned}$$

Provided with all the form factors available from the interactions, we can eliminate some of them which are apparently unfavorable energetically.

In this minimal model for KFe₂As₂, within the AB layer there is only a small hole pocket around Γ point. The Cooper pair formed on the FS is more likely to be scattered onto the same FS with small momentum transfer. And the pairing interactions $J_1(q) \propto -2J_1(\cos q_x + \cos q_y)$ and $J_{2s}(q) \propto -4J_{2s} \cos q_x \cos q_y$ are attractive when $q \approx 0$, while $J_{2d}(q) \propto 4J_{2d} \sin q_x \sin q_y$ tends to vanish. Therefore, the pairing components Δ_{1d} and Δ_{2d} are energetically unfavorable compared to Δ_{1s} and Δ_{2s} , which endow the FS with largest possible energy gain. In fact, we did some self-consistent calculation numerically to verify the results $\Delta_{1d} = \Delta_{2d} = 0$. Thus we are left with two *s*-wave pairing components Δ_{1s} and Δ_{2s} to be determined self-consistently by minimizing the ground state energy.

As there is only single hole pocket FS in the low energy excitations, we can project the effective Hamiltonian onto the hole band and especially focus on the vicinity of FS. Turned to the band basis $\Gamma_{\mathbf{k},\sigma} \equiv (\alpha_{\mathbf{k},\sigma}, \beta_{\mathbf{k},\sigma})^T$, the mean-field Hamiltonian can be straightforwardly obtained

$$\begin{aligned}H_{\text{eff}}^{\text{ab}} &= \frac{1}{2} \sum_{\mathbf{k},\sigma} \xi_h(\mathbf{k}) \beta_{\mathbf{k},\sigma}^\dagger \beta_{\mathbf{k},\sigma} \\ &+ \frac{1}{2} \sum_{\mathbf{k}} \left(\Delta_0(\mathbf{k}) - \frac{i\epsilon_{xd}(\mathbf{k})\Delta_x(\mathbf{k})}{\sqrt{\epsilon_{xd}^2 + \epsilon_z^2}} \right) \beta_{\mathbf{k},\uparrow}^\dagger \beta_{-\mathbf{k},\downarrow}^\dagger + h.c..\end{aligned}\quad (10)$$

Here we can see that the *s*-wave pairing component Δ_x arising from the NN spin exchange interaction is renormalized by a *d*-wave form factor $\epsilon_{xd} \propto (\cos k_x - \cos k_y)$, which is inherited from the NN hopping integral in the C_4^p symmetry representation. Actually it should be no surprise, since we can physically understand this renormalization factor in the following way. The NN pairing interaction glues the inter-sublattice particles, which coexist in the hole band with probability proportional to the hybridization energy gain. As a result, the effective intra-hole-band pairing condensate is supposed to be renormalized by ϵ_{xd} . As shown in Fig.1c, along the zero lines of hybridization energy ϵ_{xd} , there is no coexistence of the sublattice degrees of freedom so that there are no inter-orbital Cooper pairs, regardless of their internal pairing symmetry. Such a mechanism is parallel to the effective intra-band *p*-wave pairing induced on the helical electrons in proximity to the *s*-wave superconductors[38].

Then the Bogoliubov quasi-particle spectrum can be derived

$$E(\mathbf{k}) = \pm \sqrt{\xi_h^2(\mathbf{k}) + \Delta_0^2(\mathbf{k}) + \tilde{\Delta}_x^2(\mathbf{k})}, \quad (11)$$

where $\tilde{\Delta}_x(\mathbf{k}) \equiv \frac{\epsilon_{xd}(\mathbf{k})}{\sqrt{\epsilon_{xd}^2 + \epsilon_z^2}} \Delta_x(\mathbf{k})$ and $E(\mathbf{k})$ exhibits the nodal excitations when $\Delta_0(\mathbf{k}) = 0$. Note that the inter-band pairing between hole band and high energy electron band only contributes second order perturbation corrections to the gap structure, but is unable to alter its symmetry. The *d*-wave gap nodes carrying one unit of vorticity in the Nambu space are topologically protected[42, 43]. Within the AB layer, there are only two ways to destroy these nodes. The first one is to generate a mass upon the massless Bogoliubov quasi-particles[44] which is forbidden by the TR symmetry in pairing sector. The mass term is an additional pairing component with phase difference that cannot be gauged away. The other way is to move the nodes with opposite vorticity to annihilate each other, which is prevented by the C_4^p symmetry that confines the nodes to the unfolded BZ diagonal.

Now we have two competing pairing components: the NNN Cooper pair condensate $\Delta_0(\mathbf{k})$ with the $s_{x^2y^2}$ -wave form factor and the NN Cooper pair condensate $\tilde{\Delta}_x(\mathbf{k})$ carrying the $d_{x^2-y^2} \times s_{x^2+y^2}$ -wave form factor. They can be varied by the NN interaction J_1 for a fixed NNN interaction $J_{2s} \simeq 0.3$. The detailed self-consistency calculation explicitly shows phase transitions of pairing symmetry displayed in Fig.3. When $J_1 \ll J_{2s}$, the NNN interaction overwhelms the NN interaction, leading to the $s_{x^2y^2}$ -wave pairing, whereas $J_1 \gg J_{2s}$ results in the $d_{x^2-y^2} \times s_{x^2+y^2}$ -wave pairing. In between, the SC with a mixed pairing $s + id \times s$ is energetically more favorable, which spontaneously breaks the TR symmetry. To compare with the pressure experiments[32], we notice that, upon increasing pressure, both t_2 and J_2 are expected to grow faster than t_1 and J_1 . Since the dopant concentration is fixed and the small hole pocket FS does not change qualitatively, we expect that decreasing the ratio of J_1/J_{2s} is adequate to capture the essential physics during the period of increasing pressure. When the superfluid density does not vary drastically, the superconducting critical temperature would be roughly proportional to the maximum gap on the FS, and it turns out the tendency of maximum gap on the FS along J_1 shown by the black solid line in Fig.3 concurs qualitatively well with the T_c trend under decreasing pressure in experiments[32]. Moreover, the phase transition from the $d \times s$ -wave nodal SC to the $s + id \times s$ nodeless SC belongs to the TR breaking mass generation scenario of destroying the pairing gap nodes.

For the CD layer, we can simply apply the S_4 symmetry to obtain its low-energy effective Hamiltonian:

$$\begin{aligned}H_{\text{eff}}^{\text{cd}} &= \frac{1}{2} \sum_{\mathbf{k},\sigma} \xi_h(\mathbf{k}) \gamma_{\mathbf{k},\sigma}^\dagger \gamma_{\mathbf{k},\sigma} \\ &+ \frac{\eta}{2} \sum_{\mathbf{k}} \left(\Delta_0(\mathbf{k}) + \frac{\epsilon_{xd}(\mathbf{k})}{\sqrt{\epsilon_{xd}^2 + \epsilon_z^2}} i\Delta_x(\mathbf{k}) \right) \gamma_{\mathbf{k},\uparrow}^\dagger \gamma_{-\mathbf{k},\downarrow}^\dagger + h.c.\end{aligned}\quad (12)$$

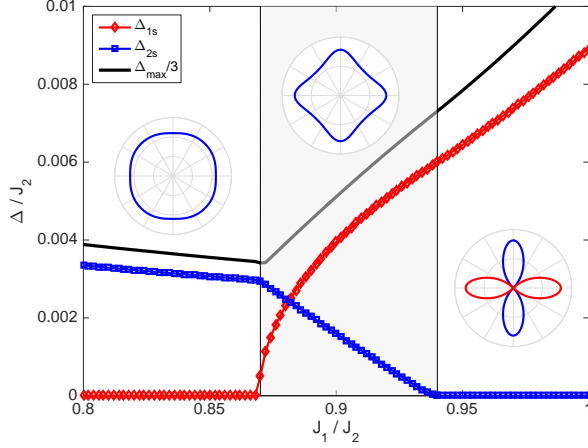


FIG. 3: Phase diagram of the superconducting phases for KFe₂As₂ under pressure (decreasing J_1 mimics the trend of increasing pressure). The parameters are $x = 0.05$, $t_{1d} = -1.2$, $t_{2s} = 0.5$, $J_2 = 0.5$, $J'_2 = 0.2$ in unit of $t_{2d} = 1$. Red line is for the NN Cooper pair $|\Delta_{1s}|$ that obtains $s_{x^2y^2}$ form factor in momentum space, while blue line is for the NNN Cooper pair condensate $|\Delta_{2s}|$ who is endowed with $d_{x^2-y^2} \times s_{x^2+y^2}$ -wave form factor. The $d_{x^2-y^2} \times s_{x^2+y^2}$ -wave SC comes to replace the $s_{x^2y^2}$ -wave SC when J_1 overwhelms J_{2s} . The grey color region marks the intermediate phase region with $s_{x^2y^2} + id_{x^2-y^2} \times s_{x^2+y^2}$ mixed pairing SC. Black solid line shows the maximal gap along the FS, which is roughly proportional to the critical temperature when superfluid density does not vary drastically. Insets show the pairing gap structure on the FS, characteristic of the three pairing phases, respectively.

where $\gamma_{\mathbf{k},\sigma}^\dagger = (\cos \frac{\theta_{\mathbf{k}}}{2}) c_{\mathbf{k},\sigma}^\dagger - \text{sgn}(\epsilon_{xd}) (\sin \frac{\theta_{\mathbf{k}}}{2}) d_{\mathbf{k},\sigma}^\dagger$. η embodies the global phase difference between the pairing condensates of the two layers, and is restricted to be either ± 1 or $\pm i$ as the one-dimensional representations of the S_4 point group[22]. The relative phase difference can be pinned down by inter-layer couplings for the benefit of energetics.

Octet nodal SC from distorting d -wave pairing

We are now in a good position to focus on the nodal phase at ambient pressure, which appears like a sphinx in a variety of experiments. Based on what we obtained, we have two S_4 -related C_4^p symmetric hole pockets which are absolutely degenerate. They can form d -wave pairing condensates with degenerate quartet nodes residing on the unfolded BZ diagonal (Fig.4a and 4b). Such degeneracy is highly unstable against any arbitrary perturbation, so we are obliged to return to the more realistic materials by involving the weak C_4^p -breaking hopping t_{1s} and inter-layer tunneling t_c . As for the inter-layer tunneling, the s -wave NN tunneling would be the dominant term, from the estimate of orbitals overlap and symmetry analysis (see Fig.1b). Note that the on-site tunneling is suppressed because of the orbital orthogonality. Surprisingly, the S_4 symmetry survives this tunneling process. When $t_c \ll t_{1s} \ll t_{1d}$, the effective Hamiltonians for the AB and CD layers are modified by t_{1s} in their respective

ways:

$$H_{\text{eff}}^{\text{ab}} \rightarrow \frac{1}{2} \sum_{\mathbf{k},\sigma} \xi_h^+(\mathbf{k}) \beta_{\mathbf{k},\sigma}^\dagger \beta_{\mathbf{k},\sigma} \quad (13)$$

$$+ \frac{1}{2} \sum_{\mathbf{k}} \frac{\epsilon_{xd}(\mathbf{k}) + \epsilon_{xs}(\mathbf{k})}{\sqrt{(\epsilon_{xd} + \epsilon_{xs})^2 + \epsilon_z^2}} \Delta_x(\mathbf{k}) \beta_{\mathbf{k},\uparrow}^\dagger \beta_{-\mathbf{k},\downarrow}^\dagger + h.c.$$

$$H_{\text{eff}}^{\text{cd}} \rightarrow \frac{1}{2} \sum_{\mathbf{k},\sigma} \xi_h^-(\mathbf{k}) \gamma_{\mathbf{k},\sigma}^\dagger \gamma_{\mathbf{k},\sigma} \quad (14)$$

$$+ \frac{\eta}{2} \sum_{\mathbf{k}} \frac{-\epsilon_{xd}(\mathbf{k}) + \epsilon_{xs}(\mathbf{k})}{\sqrt{(\epsilon_{xd} - \epsilon_{xs})^2 + \epsilon_z^2}} \Delta_x(\mathbf{k}) \gamma_{\mathbf{k},\uparrow}^\dagger \gamma_{-\mathbf{k},\downarrow}^\dagger + h.c.$$

where the global phase of Δ_{1s} has been gauged to absorb the phase factor $-i$. Meanwhile, the normal state dispersion and the hybridization angle for AB/CD layer are given by

$$\xi_h^\pm(\mathbf{k}) = \epsilon_0(\mathbf{k}) - \sqrt{(\epsilon_{xd} \pm \epsilon_{xs})^2 + \epsilon_z^2}, \quad (15)$$

and $\theta^\pm = \tan^{-1} \frac{|\epsilon_{xd} \pm \epsilon_{xs}|}{\epsilon_z}$, so that the quasiparticles, $\beta_{\mathbf{k},\sigma}^\dagger$ and $\gamma_{\mathbf{k},\sigma}^\dagger$ are adapted (see Supplementary Material for detail). As a result, the d -wave nodal lines that used to lie across the unfolded BZ diagonal are now twisted and dragged away from the Γ point by a "nematic force", resulting in a simultaneous movement of nodes along the elongating direction of the hole Fermi pockets (Fig.4a and 4b). Since the nodes with opposite vorticity need to travel a finite path along the FS before annihilation, they can survive a finite weak C_4^p -breaking term depending on the size of the FS.

The hole pockets from the AB and CD layers are required by S_4 symmetry to intersect at the unfolded BZ diagonal (Fig.4c). Degeneracy at this point is unstable against any arbitrarily weak perturbation of inter-layer tunneling:

$$H_c = \frac{1}{2} \sum_{\mathbf{k},\sigma} \left[\epsilon_c(\mathbf{k}) (a_{\mathbf{k},\sigma}^\dagger d_{\mathbf{k},\sigma} + b_{\mathbf{k},\sigma}^\dagger c_{\mathbf{k},\sigma}) + h.c. \right] \rightarrow \frac{1}{2} \sum_{\mathbf{k},\sigma} \left[\tilde{\epsilon}_c(\mathbf{k}) \beta_{\mathbf{k},\sigma}^\dagger \gamma_{\mathbf{k},\sigma} + h.c. \right]. \quad (16)$$

So the degenerate Fermi-points at the unfolded BZ diagonal are split by $\tilde{\epsilon}_c(\mathbf{k})$ into two Fermi-points, whose corresponding quasi-particles are given by the bonding and anti-bonding states of the two layers. The split Fermi points smoothly join the Fermi sheets far away from the unfolded BZ diagonal, where $\tilde{\epsilon}_c(\mathbf{k})$ amounts only up to second order perturbation corrections (Fig.4c). Next let's consider how the pairing matrix changes with the inter-layer tunneling. It is expected that $\eta = 1$ to avoid the destructive interference along the BZ diagonal where two layers strongly hybridize. Therefore, the pairing condensates on the unfolded BZ diagonal were identical for hole pockets from both layers, guaranteed by the S_4 symmetry

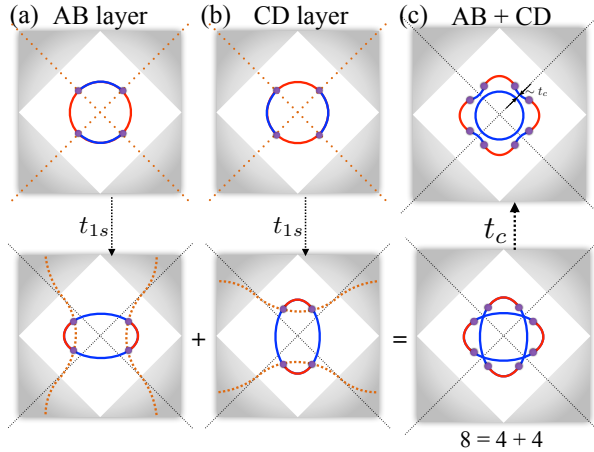


FIG. 4: Distorted d -wave nodes on the Fermi surfaces. The white diamond emphasizes the folded BZ; the orange dashed lines denote the nodal lines of the effective $d_{x^2-y^2}$ -wave pairing condensate on the FS distorted by $s_{x^2+y^2}$ -wave factor (the effect of weak s -wave is moderately exaggerated for illustration); The FS is separated by pairing nodal lines into the segments with positive (negative) pairing condensate marked by red (blue) color, respectively. (a) In the AB layer, the mixing weak s -wave NN hopping acts like a "nematic force" that elongates the FS and distorts the d -wave nodal lines, leading to shifted quartet nodes. (b) As the CD layer is related to AB layer by the S_4 symmetry, the distortion occurs in the perpendicular direction. (c) Near unfolded BZ diagonal the quasi-particles from the AB and CD layers are strongly hybridized with each other by any infinitesimal inter-layer tunneling. The intersecting elliptic hole pockets are therefore reconstructed into inner and outer pockets. The inner one has nodeless pairing gap whereas the outer one shows octet nodal gap structure. The origin of nodes can be attributed to a rather simple symbolic equation "8=4+4".

(Fig.4c). The bonding of the two layers does not affect the pairing matrix along unfolded BZ diagonal, which maintains diagonal in the form of identity (see Supplementary Material for detail). As a result, the two reconstructed bands yield the outer and inner hole pockets and are decoupled in pairing sector to the leading order. The outer pocket inherits the total octet nodes (Fig.4c), which still carry vorticity in the Nambu space and are protected by topology. On the inner pocket the pairing gap is nodeless. It should be made clear that our outer pocket corresponds to the "middle pocket" termed in experimental report[30], because the d_{xy} orbital has been neglected in our minimal model.

In this picture, we have seen how the octet nodes come out naturally as observed in the laser ARPES[30], and we can understand why every two of the octet nodes are located so close to the unfolded BZ diagonal in experiment, because they are essentially born of the d -wave representation of C_4^p albeit distorted by the weak C_4^p -breaking term. Therefore, the so-called "octet-noded monster" is neither accidental nor some crazy Cooper pair of angular

momentum as high as g -wave, but the combination of two distorted d -wave related by the S_4 symmetry. In short, the origin of nodes can be attributed to a symbolic equation "8 = 4+4". The nodes share the same fate with the FS structure that protests against strong breaking of C_4^p symmetry. Therefore, we settle the disagreement between d -wave gap structure and the observation of octet nodes on one of the hole pockets. All in all, the key feature lies in the multi-orbital character.

DISCUSSION

Inspired by this organizing principle governed by C_4^p and S_4 symmetries, we can gain some insight into the electronic structure and pairing symmetry of iron-selenide (FeSe). While the d -wave representation C_4^p of plaquette-centered rotation symmetry stabilizes the FS structure of iron-pnictides, the s -wave representation \tilde{C}_4^p captures the key feature of FSs in FeSe as shown in Fig.5a, where the NN s -wave hopping dominates. In Fig.5b, it can be shown that, when the d -wave NN hopping is completely replaced by the s -wave hopping followed by a particle-hole transform, we can obtain the FS with a robust electron pocket around X point without hole pocket around Γ point, which is characteristic of FeSe[41]. In this case, the electron pocket and its central double Dirac point are protected by the TR symmetry together with the s -wave representation of the plaquette-centered rotation symmetry $\tilde{C}_4^p \equiv \tau_{31}$. Thus, the band structure of FeSe is related to that of iron-pnictides by a gauge transform combined with a particle-hole transform.

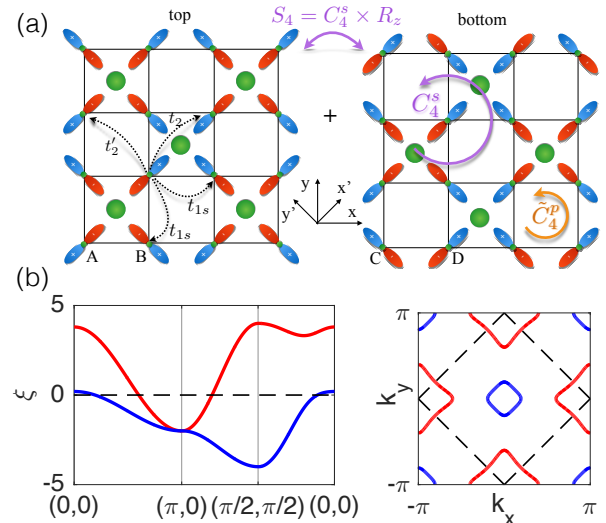


FIG. 5: (a) Gauge choice characteristic of FeSe, followed by a particle-hole transform. (b) Band dispersion typical of iron-chalcogenides, where the electron pocket around $(\pi,0)$ is robust while hole pocket around $(0,0)$ is dispensable. The parameters for the demonstration are chosen to be $t_{1d} = 0$, $t_{1s} = 0.45$, $t_{2s} = 0.5$ in unit of $t_{2d} = 1$.

When the pairing symmetry is considered, we can just focus on the monolayer FeSe with only electron Fermi pockets around X point[41]. Parallel to the above discussion for KFe_2As_2 , there are two possible pairing symmetries for the monolayer FeSe: one is the $s_{x^2-y^2}$ -wave Cooper pair glued by the dominant NNN AF coupling J_2 and the other one is the effective $s_{x^2+y^2} \times d_{x^2-y^2}$ -wave Cooper pair on the electron pockets around the X point for a relatively large NN AF coupling J_1 . Although the inter-orbital Cooper pairs glued by J_1 has $d_{x^2-y^2}$ -wave symmetry, whose nodal line avoids the FS to maximize the energy gain, the projection of the inter-orbital Cooper pairs onto the FS yields an additional $s_{x^2+y^2}$ form factor inherited from the electronic structure. However, when J_2 overwhelms J_1 , the pairing symmetry is the $s_{x^2-y^2}$ -wave. Without more interactions, the two layers tolerating weak inter-layer tunneling tend to lock their respective phases of Cooper pairs to be identical, otherwise there would be destructive interference. This supports the plain s-wave pairing symmetry as observed by the STM measurement[45]. But when J_1 dominates over J_2 , the effective $s_{x^2+y^2} \times d_{x^2-y^2}$ -wave pairing condensate would show a gap minimum near the folded BZ boundary and a gap maximum along the unfolded BZ boundary, which seems to concur with the superconducting gap anisotropy measured by ARPES[41].

[1] J. P. Bednorz and K. A. Muller, Possible high-Tc superconductivity in the Ba-La-Cu-O system, *Z. Phys. B* **64**, 189 (1986).

[2] P. W. Anderson, The resonating valence bond state in La_2CuO_4 and superconductivity, *Science* **235**, 1196 (1987).

[3] P. W. Anderson, P. A. Lee, M. Randeria, T. M. Rice, N. Trivedi, and F. C Zhang, The physics behind high-temperature superconducting cuprates: The "plain vanilla" version of RVE, *J. Phys. Condens. Matter* **16**, R755 (2004).

[4] P. A. Lee, N. Nagaosa, and X. G. Wen, Doping a Mott insulator: physics of high temperature superconductivity, *Rev. Mod. Phys.* **78**, 17 (2006).

[5] Z. X. Shen, D. S. Dessau, B. O. Wells, D. M. King, W. E. Spicer, A. J. Arko, D. Marshall, L. W. Lombardo, A. Kapitulnik, P. Dickinson, S. Doniach, J. DiCarlo, T. Loeser, and C. H. Park, Anomalously large gap anisotropy in the a-b plane of $Bi_2Sr_2CaCu_2O_{8+\delta}$, *Phys. Rev. Lett.* **70**, 1553 (1993).

[6] D. A. Wollman, D. J. Van Harlingen, W. C. Lee, D. M. Ginsberg, and A. J. Leggett, Experimental determination of the superconducting pairing state in YBCO from the phase coherence of YBCO-Pb dc SQUIDs, *Phys. Rev. Lett.* **71**, 2134 (1993).

[7] C. C. Tsuei, J. R. Kirtley, C. C. Chi, L. S. Yujahnes, A. Gupta, T. Shaw, J. Z. Sun, and M. B. Ketchen, Pairing symmetry and flux quantization in a tricrystal superconducting ring of $YBa_2Cu_3O_{7-\delta}$, *Phys. Rev. Lett.* **73**, 593 (1994).

[8] F. C. Zhang, and T. M. Rice, Effective Hamiltonian for the superconducting Cu oxides, *Phys. Rev. B* **37**, 3759 (1988).

[9] G. Kotliar and J. Liu, Superexchange mechanism and d-wave superconductivity, *Phys. Rev. B* **38**, 5142 (1988).

[10] B. E. C. Koltenbah and R. Joynt, Material-specific gap function in the high-temperature superconductors, *Rep. Prog. Phys.* **60**, 23 (1997) and references therein.

[11] J. Paglione and R. L. Greene, High-temperature superconductivity in iron-based materials, *Nat. Phys.* **6**, 645 (2010).

[12] I. I. Mazin, Superconductivity gets an iron boost, *Nature (London)* **464**, 183 (2010).

[13] D. N. Basov and A. V. Chubukov, Manifesto for a higher T_c – lessons from pnictides and cuprates, *Nat. Phys.* **7**, 272 (2011).

[14] P. J. Hirschfeld, M. M. Korshunov, and I. I. Mazin, Gap symmetry and structure of Fe-based superconductors, *Rev. Prog. Phys.* **74**, 124508 (2011).

[15] A. V. Chubukov, Pairing mechanism in Fe-based superconductors, *Annu. Rev. Condens. Matter Phys.* **3**, 57 (2012).

[16] R. M. Fernandes, A. V. Chubukov, and J. Schmalian, Nematic order in iron superconductors - who is in the driver's seat?, *Nat. Phys.* **10**, 97 (2014).

[17] T. Terashima, M. Kimata, N. Kurita, H. Satsukawa, A. Harada, K. Hazama, M. Imai, A. Sato, K. Kihou, C.-H. Lee, H. Kito, H. Eisaki, A. Iyo, T. Saito, H. Fukazawa, Y. Kohori, H. Harima, and S. Uji, Fermi surface and mass enhancement in KFe_2As_2 from de Haas-van Alphen effect measurements, *J. Phys. Soc. Jpn.* **79**, 053702 (2010).

[18] T. Sato, K. Nakayama, Y. Sekiba, P. Richard, Y.-M. Xu, S. Souma, T. Takahashi, G. F. Chen, J. L. Luo, N. L. Wang, and H. Ding, Band Structure and Fermi Surface of an Extremely Overdoped Iron-Based Superconductor KFe_2As_2 , *Phys. Rev. Lett.* **103**, 047002 (2009).

[19] S. Graser, T. A. Maier, P. J. Hirschfeld, and D. J. Scalapino, Near-degeneracy of several pairing channels in multiorbital models for the Fe-pnictides, *New J. Phys.* **11**, 025016 (2009).

[20] K. J. Seo, B. A. Bernevig and J. Hu, Pairing symmetry in a two-orbital exchange coupling model of oxypnictides, *Phys. Rev. Lett.* **101**, 206404 (2008).

[21] R. Yu, J. Zhu, and Q. Si, Mott Transition in modulated lattices and parent insulator of $(K,Tl)_yFe_xSe_2$, superconductors, *Phys. Rev. Lett.* **106**, 186401 (2011).

[22] J. Hu and N. Hao, S_4 symmetric microscopic model for iron-based superconductors, *Phys. Rev. X* **2**, 021009 (2012).

[23] J. K. Dong, S. Y. Zhou, T. Y. Guan, H. Zhang, Y. F. Dai, X. Qiu, X. F. Wang, Y. He, X. H. Chen, and S. Y. Li, Quantum criticality and nodal superconductivity in the FeAs-based superconductor KFe_2As_2 , *Phys. Rev. Lett.* **104**, 087005 (2010).

[24] K. Hashimoto, A. Serafin, S. Tonegawa, R. Katsumata, R. Okazaki, T. Saito, H. Fukazawa, Y. Kohori, K. Kihou, C. H. Lee, A. Iyo, H. Eisaki, H. Ikeda, Y. Matsuda, A. Carrington, and T. Shibauchi, Evidence for superconducting gap nodes in the zone-centered hole bands of KFe_2As_2 from magnetic penetration-depth measurements, *Phys. Rev. B* **82**, 014526 (2010).

[25] H. Fukazawa, Y. Yamada, K. Kondo, T. Saito, Y. Kohori, K. Kuga, Y. Matsumoto, S. Nakatsuji, H. Kito, P.M. Shirage, K. Kihou, N. Takeshita, C.-H. Lee, A. Iyo, and

H. Eisaki, Possible multiple gap superconductivity with line nodes in heavily hole-doped superconductor KFe_2As_2 studied by ^{75}As -NQR and specific heat, *J. Phys. Soc. Jpn.* **78**, 083712 (2009).

[26] S. W. Zhang, L. Ma, Y. D. Hou, J. Zhang, T. -L. Xia, G. F. Chen, J. P. Hu, G. M. Luke, and W. Yu, ^{75}As NMR study of single crystals of the heavily overdoped pnictide superconductors $Ba_{1-x}K_xFe_2As_2$ ($x=0.7$ and 1), *Phys. Rev. B* **81**, 012503 (2010).

[27] Y. P. Wu, D. Zhao, A. F. Wang, N. Z. Wang, Z. J. Xiang, X. G. Luo, T. Wu, and X. H. Chen, Emergent Kondo lattice behavior in iron-based superconductors AFe_2As_2 ($A=K, Rb, Cs$), *Phys. Rev. Lett.* **116**, 147001 (2016).

[28] R. Thomale, C. Platt, W. Hanke, J. Hu and B. A. Bernevig, Exotic d-wave superconducting state of strongly hole-doped $K_xBa_{1-x}Fe_2As_2$, *Phys. Rev. Lett.* **107**, 117001 (2011).

[29] J. P. Reid, M. A. Tanatar, A. Juneau-Fecteau, R. T. Gordon, S. Rende Cotret, N. Doiron-Leyraud, T. Saito, H. Fukazawa, Y. Kohori, K. Kihou, C. H. Lee, A. Iyo, H. Eisaki, R. Prozorov, and Louis Taillefer, Universal heat conduction in the iron arsenide superconductor KFe_2As_2 : Evidence of a d-wave state, *Phys. Rev. Lett.* **109**, 087001 (2012).

[30] K. Okazaki, Y. Ota, Y. Kotani, W. Malaeb, Y. Ishida, T. Shimojima, T. Kiss, S. Watanabe, C.-T. Chen, K. Kihou, C. H. Lee, A. Iyo, H. Eisaki, T. Saito, H. Fukazawa, Y. Kohori, K. Hashimoto, T. Shibauchi, Y. Matsuda, H. Ikeda, H. Miyahara, R. Arita, A. Chainani and S. Shin, Octet-line node structure of superconducting order parameter in KFe_2As_2 , *Science* **337** (6100), 1314-1317 (2012).

[31] T. Ong, P. Coleman, and J. Schmalian, Concealed d-wave pairs in the s^\pm condensate of iron-based superconductors, *PNAS* **113**, 5486-5491 (2016).

[32] F. F. Tafti, A. Juneau-Fecteau, M. E Delage, S. Rene de Cotret, J. P. Reid, A. F. Wang, X. G. Luo, X. H. Chen, N. Doiron-Leyraud and L. Taillefer, Change of pairing symmetry in the iron-based superconductor KFe_2As_2 , *Nature Physics* **9**, 349-352 (2013).

[33] F. Hardy, A. E. Boehmer, D. Aoki, P. Burger, T. Wolf, P. Schweiss, R. Heid, P. Adelmann, Y. X. Yao, G. Kotliar, J. Schmalian, and C. Meingast, Evidence of strong correlations and coherence-incoherence crossover in the iron pnictide superconductor KFe_2As_2 , *Phys. Rev. Lett.* **111**, 027002 (2013).

[34] M. Nakajima, S. Ishida, T. Tanaka, K. Kihou, Y. Tomioka, T. Saito, C. -H. Lee, H. Fukazawa, Y. Kohori, T. Kakeshita, A. Iyo, T. Ito, H. Eisaki, and S. Uchida, Strong electronic correlations in iron pnictides: Comparison of the optical spectra for $BaFe_2As_2$ -related compounds, *J. Phys. Soc. Jpn.* **83**, 104703 (2014).

[35] V. Cvetkovic and O. Vafek, Space group symmetry, spin-orbit coupling, and the low-energy effective Hamiltonian for iron-based superconductors, *Phys. Rev. B* **88**, 134510 (2013).

[36] D. Liu, W. Zhang, D. Mou, J. He, Y.-B. Ou, Q.-Y. Wang, Z. Li, L. Wang, L. Zhao, S. He, Y. Peng, X. Liu, C. Chen, L. Yu, G. Liu, X. Dong, J. Zhang, C. Chen, Z. Xu, J. Hu, X. Chen, X. Ma, Q. Xue, X. J. Zhou, Electronic origin of high temperature superconductivity in single-layer FeSe superconductor, *Nature Commun.* **3**, 931 (2012).

[37] S. Y. Tan, M. Xia, Y. Zhang, Z. R. Ye, F. Chen, X. Xie, R. Peng, D. F. Xu, Q. Fan, H. C. Xu, J. Juan, T. Zhang, X. C. Lai, T. Xiang, J. P. Hu, B. P. Xie, D. L. Feng, Interface-induced superconductivity and strain-dependent spin density wave in $FeSe/SrTiO_3$ thin films, *Nature Mater.* **12**, 634 (2013).

[38] L. Fu and C. L. Kane, Superconducting proximity effect and majorana Fermions at the surface of a topological insulator, *Phys. Rev. Lett.* **100**, 096407 (2008).

[39] V. Grinenko, P. Materne, R. Sarkar, H. Luetkens, K. Kihou, C. R. Lee, S. Akhmadaliev, D. V. Efremov, S. L. Drechsler, and H. H. Klauss, Superconductivity with broken time-reversal symmetry in ion-irradiated $Ba_{0.27}K_{0.73}Fe_2As_2$ single crystals, *Phys. Rev. B* **95**, 214511 (2017).

[40] Y. Ran, F. Wang, H. Zhai, A. Vishwanath, and D. -H. Lee, Nodal spin density wave and band topology of the FeAs-based materials, *Phys. Rev. B* **79**, 014505 (2009).

[41] Y. Zhang, J. J. Lee, R. G. Moore, W. Li, M. Yi, M. Hashimoto, D. H. Lu, T. P. Devereaux, D. H. Lee and Z. X. Shen, Superconducting gap anisotropy in monolayer FeSe thin film, *Phys. Rev. Lett.* **117**, 117001 (2016).

[42] F. Wang and D. -H. Lee, Topological relation between bulk gap nodes and surface bound states: Application to iron-based superconductors, *Phys. Rev. B* **86**, 094512 (2012).

[43] G. Y. Zhu, G. M. Zhang, Topological phase transition from nodal to nodeless d-wave superconductivity in electron-doped cuprate superconductors, *Europhys. Lett.* **117**, 67007 (2017).

[44] G. Y. Zhu, Z. Wang, G. M. Zhang, Two-dimensional topological superconducting phases emerged from d-wave superconductors in proximity to antiferromagnets, *Europhys. Lett.* **118**, 37004 (2017).

[45] Q. Fan, W. H. Zhang, X. Liu, Y. J. Yan, M. Q. Ren, R. Peng, H. C. Xu, B. P. Xie, J. P. Hu, T. Zhang and D. L. Feng, Plain s-wave superconductivity in single-layer FeSe on $SrTiO_3$ probed by scanning tunneling microscopy, *Nature Physics* **11**, 946-952 (2015).

Acknowledgment

GMZ acknowledges the support of National Key Research and Development Program of China (2016YFA0300300).

Author contributions

GMZ initiated and supervised this project, GYZ conducted the derivation and calculation, and GYZ and GMZ wrote the paper.